Variational analysis of the natural decay rates and eigenmodes of cavity-enclosed diffusive fields

2007 J. Phys. A: Math. Theor. 40 12463

(http://iopscience.iop.org/1751-8121/40/41/014)

IOP PUBLISHING JOURNAL OF PHYSICS A: MATHEMATICAL AND THEORETICAL

J. Phys. A: Math. Theor. **40** (2007) 12463–12477 doi:10.1088/1751-8113/40/41/014

Variational analysis of the natural decay rates and eigenmodes of cavity-enclosed diffusive fields

Adrianus T de Hoop[1] **and Michael D Prange**

Schlumberger-Doll Research, One Hampshire Street, Cambridge, MA 02139-1578, USA

E-mail: a.t.dehoop@ewi.tudelft.nl and prange@slb.com

Received 8 May 2007, in final form 31 July 2007
Published 25 September 2007
Online at stacks.iop.org/JPhysA/40/12463

Abstract

A variational approach to the analysis of the natural decay rates and eigenmodes of cavity-enclosed diffusive fields in general anisotropic and heterogeneous materials is presented. In the bulk material, diffusivity and volume relaxivity are accounted for. The interaction of the cavity's medium with the embedding material is modeled via a surface relaxivity on the boundary surface. The pertaining eigenmodes are proven to be orthogonal and to form a complete expansion of an initially excited diffusive field. In view of the variational approach, a finite-element type of computation presents itself as the natural tool for numerics. The resulting implementation on a simplicial mesh allows for the modeling of cavities of arbitrary shape. To investigate the feasibility of using the approach in the inverse problem of reconstructing the shape and size of cavities from measured values of the natural decay rates of the eigenmodes, we carry out a number of numerical experiments on the forward problem. They demonstrate the method to be simple and robust, both in 2D and 3D complex geometries. For a benchmark problem with a known analytic solution, error estimates are presented. Applications are found in, for example, nuclear magnetic resonance imaging of subsurface rock pore geometry, biological cell structure and the analysis of neurological defects in medical diagnostics.

PACS number: 82.56.Lz

1. Introduction

This paper deals with the eigenmodes and their natural decay rates of cavity-enclosed diffusive fields. In particular, the stationarity properties (in the sense of variational calculus) of the natural decay rates are discussed. From them, a procedure is constructed that leads to the

[1] Visiting from Laboratory of Electromagnetic Research, Faculty of Electrical Engineering, Mathematics and Computer Science, Delft University of Technology, Mekelweg 4, 2628 CD Delft, The Netherlands.

computation of these decay rates as well as of the spatial distribution of the corresponding eigenmodes over the region occupied by the cavity. Volume or bulk relaxivity of the medium in the cavity, as well as surface relaxivity on its boundary to model the diffusive interaction with the cavity's embedding, are taken into account. General inhomogeneous and anisotropic diffusion are considered.

Although the diffusion problem under consideration is formulated quite generally, it is mainly inspired by NMR experiments that are designed to extract configurational information about objects under interrogation. We mention such diverse applications as pore size and pore shape distribution in subsurface hydrocarbon reservoirs in the Earth, cell biology and neuroimaging in medical diagnostics, references to which can be found in recent tutorial papers [1, 2]. These experiments use applied and internal magnetic field gradients to initialize the spatially varying distributions of the spin magnetization. Subsequently, they monitor the evolution (often decay) of the spatial modulation as a function of diffusion time and in dependence on the spatial patterns. These techniques have allowed measurements of fundamental geometric parameters of the pore network, such as surface-to-volume ratio and pore sizes. It would be highly desirable to extend these methods to obtain more detailed information on pore geometry, such as pore shape, pore–pore distance and pore connectivity. Such properties are embedded in the diffusive eigenmodes that are the focus of this paper. The availability of a high-speed computer algorithm to solve the associated forward problem for arbitrary pore shapes will be critical in guiding further experimental development. The stationarity property of the natural decay rates of the cavity modes provides the basis for a highly effective finite-element type of algorithm that allows for the generation of data for cavity shapes that are not amenable to analytic methods (such as spheres and circular cylinders).

For NMR imaging of cavity size and shape, it is desirable to represent the diffusive field of the spin magnetization in terms of a small number of eigenmodes [2]. As stated above, eigenmodes, and their decay rates, for simple pore shapes can be calculated analytically [3, 4], but pores in natural materials are mostly of irregular shapes. One approach to evaluate the eigenmodes in such a case is to express the diffusion equation in the time Laplace-transform domain (see equation (19)) and then make a finite-difference approximation of the spatial differential operator on a rectangular grid [5]. This procedure results in a standard matrix eigenproblem that can efficiently be solved by standard methods. The disadvantage of this approach comes with irregular shapes, where the necessity to express the boundary conditions accurately on a rectangular finite-difference grid leads to excessive grid refinement and thus to an excessive increase in computation time. The method that we present is based on the physical property of stationarity of the natural decay rates and is thus of a variational nature. Computationally, it leads to an algorithm of the finite-element type. Implementation of this algorithm on a simplicial, i.e., triangular (2D) or tetrahedral (3D) grid, allows for an accurate modeling of irregular boundaries without undue mesh refinement. The simplicity and the robustness of the method are illustrated by presenting results that are obtained by applying it to sample cavities of a highly irregular shape. The accuracy of the method is analyzed by comparing the numerical results with the analytical ones for a simple shape.

2. Formulation of the problem

The cavity under consideration occupies the bounded subdomain $\mathcal{D}$ of a three-dimensional space $\mathbb{R}^3$. Its closed boundary surface $\partial\mathcal{D}$ is assumed to be piecewise smooth. The outward unit vector along the normal to $\partial\mathcal{D}$ is denoted by $\boldsymbol{\nu}$. The complement of the closure of $\mathcal{D}$ in $\mathbb{R}^3$ is denoted by $\mathcal{D}'$. Position in the configuration is specified by the coordinates $\{x_1, x_2, x_3\}$ with respect to an orthogonal, Cartesian reference frame with the origin $\mathcal{O}$ and the three mutually

perpendicular base vectors $\{\boldsymbol{i}_1, \boldsymbol{i}_2, \boldsymbol{i}_3\}$ of unit length each, that, in the indicated order, form a right-handed system. The corresponding position vector is $\boldsymbol{x} = x_1\boldsymbol{i}_1 + x_2\boldsymbol{i}_2 + x_3\boldsymbol{i}_3$. The time coordinate is t. Differentiation with respect to x_m is denoted by ∂_m; ∂_t is a reserved symbol for differentiation with respect to t.

To indicate the connection with NMR experiments, we start from the Bloch equation with a constant applied background magnetic field $\boldsymbol{H}_0$ and anisotropic diffusion and spin relaxation terms included (see the classical paper by Torrey [6])

$$\partial_t \boldsymbol{M}(\boldsymbol{x},t) = \gamma \boldsymbol{M}(\boldsymbol{x},t) \times \boldsymbol{H}_0 + [\boldsymbol{\nabla}\cdot\overleftrightarrow{\boldsymbol{D}}(\boldsymbol{x})\cdot\boldsymbol{\nabla}]\boldsymbol{M}(\boldsymbol{x},t) - \overleftrightarrow{\boldsymbol{\beta}}(\boldsymbol{x})\cdot\boldsymbol{M}(\boldsymbol{x},t) \qquad \text{for} \quad \boldsymbol{x}\in\mathcal{D}, \quad t\in\mathbb{R}. \tag{1}$$

In this equation, $\boldsymbol{\nabla} = \boldsymbol{i}_1\partial_1 + \boldsymbol{i}_2\partial_2 + \boldsymbol{i}_3\partial_3$, γ is the gyromagnetic ratio, $\boldsymbol{M}(\boldsymbol{x},t)$ is the volume distribution over the cavity of the magnetization associated with the precession of spins that are excited out of their equilibrium orientation in the applied static background magnetic field, $\overleftrightarrow{\boldsymbol{D}}(\boldsymbol{x})$ is the diffusivity (or volume or bulk relaxivity), a positive definite tensor of rank 2 that takes into account the irreversible interaction of the spins with their neighbors and $\overleftrightarrow{\boldsymbol{\beta}}(\boldsymbol{x})$ is the spin relaxation tensor. In terms of the transverse and longitudinal spin relaxation rates it is given by

$$\overleftrightarrow{\boldsymbol{\beta}}(\boldsymbol{x}) = \beta_\perp(\boldsymbol{x})[\overleftrightarrow{\mathbf{1}} - \boldsymbol{i}_{H_0}\boldsymbol{i}_{H_0}] + \beta_\parallel(\boldsymbol{x})[\boldsymbol{i}_{H_0}\boldsymbol{i}_{H_0}], \tag{2}$$

where $\overleftrightarrow{\mathbf{1}}$ is the unit tensor, $\boldsymbol{i}_{H_0}$ is the unit vector along $\boldsymbol{H}_0$, $\beta_\perp(\boldsymbol{x}) > 0$ is the reciprocal of the spin relaxation time in the plane perpendicular to $\boldsymbol{H}_0$ and $\beta_\parallel(\boldsymbol{x}) > 0$ is the reciprocal of the spin relaxation time parallel to $\boldsymbol{H}_0$.

In NMR experiments, standardly the component of $\boldsymbol{M}$ parallel to $\boldsymbol{H}_0$ is measured. Denoting this component by $M = \boldsymbol{i}_{H_0}\cdot\boldsymbol{M}$, the diffusion equation for $M(\boldsymbol{x},t)$ follows from equation (1), by taking the inner product with $\boldsymbol{i}_0$, as

$$[\boldsymbol{\nabla}\cdot\overleftrightarrow{\boldsymbol{D}}(\boldsymbol{x})\cdot\boldsymbol{\nabla}]M(\boldsymbol{x},t) - \beta(\boldsymbol{x})M(\boldsymbol{x},t) - \partial_t M(\boldsymbol{x},t) = 0 \qquad \text{for} \quad \boldsymbol{x}\in\mathcal{D}, \quad t\in\mathbb{R}, \tag{3}$$

in which $\beta(\boldsymbol{x}) = \beta_\parallel(\boldsymbol{x})$. On the cavity's boundary, the diffusive field satisfies either of the boundary conditions:

Dirichlet problem:

$$M(\boldsymbol{x},t) = 0 \qquad \text{for} \quad \boldsymbol{x}\in\partial\mathcal{D}, \tag{4}$$

Neumann problem:

$$\boldsymbol{\nu}(\boldsymbol{x})\cdot\overleftrightarrow{\boldsymbol{D}}(\boldsymbol{x})\cdot\boldsymbol{\nabla}M(\boldsymbol{x},t) = 0 \qquad \text{for} \quad \boldsymbol{x}\in\partial\mathcal{D} \tag{5}$$

or

Robin problem:

$$\boldsymbol{\nu}(\boldsymbol{x})\cdot\overleftrightarrow{\boldsymbol{D}}(\boldsymbol{x})\cdot\boldsymbol{\nabla}M(\boldsymbol{x},t) + \zeta(\boldsymbol{x})M(\boldsymbol{x},t) = 0 \qquad \text{for} \quad \boldsymbol{x}\in\partial\mathcal{D}, \tag{6}$$

in which $\zeta(\boldsymbol{x}) > 0$ is the surface relaxivity (figure 1). This parameter, introduced in the classical paper by Brownstein and Tarr [3], is representative for the diffusion of spin magnetization at the boundary surface. (In [3], the parameter is denoted as the 'surface-like sink'.)

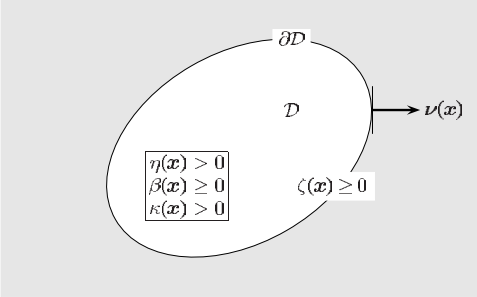

Figure 1. Cavity enclosing a diffusive field.

The natural decay rates follow from the properties of the initial-value problem, where we require

$$M(\boldsymbol{x}, t) = M_0(\boldsymbol{x}) \qquad \text{for} \quad t = 0, \quad \boldsymbol{x} \in \mathcal{D}. \tag{7}$$

The initial/boundary-value problem formulated in equations (3)–(7) has a unique solution.

In an NMR experiment, the magnetic field can be spatially varying in a porous material due to the magnetic susceptibility contrast between the solid and the pore filling liquid. Such an inhomogeneous field can significantly affect the dynamics of the transverse magnetization; however, the dynamics of the longitudinal magnetization is not affected (see equation (3)). Furthermore, this inhomogeneous field can be used to modulate the initial state of magnetization ($M_0(\boldsymbol{x})$) in an experiment, such as the DDIF experiment discussed in [7].

To arrive at an expression for the desired natural decay rates, we subject equation (3) to the Laplace transformation with respect to time:

$$\hat{M}(\boldsymbol{x}, s) = \int_{t=0}^{\infty} \exp(-st) M(\boldsymbol{x}, t)\, \mathrm{d}t \qquad \text{for} \quad s \in \mathbb{C}, \quad \mathrm{Re}(s) > 0. \tag{8}$$

This leads to

$$\begin{aligned} &\nabla \cdot [\overleftrightarrow{\boldsymbol{D}}(\boldsymbol{x}) \cdot \nabla \hat{M}(\boldsymbol{x}, s)] - \beta(\boldsymbol{x}) \hat{M}(\boldsymbol{x}, s) - s \hat{M}(\boldsymbol{x}, s) \\ &\qquad = -M_0(\boldsymbol{x}) \qquad \text{for} \quad \boldsymbol{x} \in \mathcal{D}, \quad s \in \mathbb{C}, \quad \mathrm{Re}(s) > 0, \end{aligned} \tag{9}$$

while equations (4)–(6) transform into

Dirichlet problem:

$$\hat{M}(\boldsymbol{x}, s) = 0 \qquad \text{for} \quad \boldsymbol{x} \in \partial\mathcal{D}, \quad s \in \mathbb{C}, \quad \mathrm{Re}(s) > 0, \tag{10}$$

Neumann problem:

$$\boldsymbol{\nu}(\boldsymbol{x}) \cdot \overleftrightarrow{\boldsymbol{D}}(\boldsymbol{x}) \cdot \nabla \hat{M}(\boldsymbol{x}, s) = 0 \qquad \text{for} \quad \boldsymbol{x} \in \partial\mathcal{D}, \quad s \in \mathbb{C}, \quad \mathrm{Re}(s) > 0 \tag{11}$$

and

Robin problem:

$$\boldsymbol{\nu}(\boldsymbol{x}) \cdot \overleftrightarrow{\boldsymbol{D}}(\boldsymbol{x}) \cdot \nabla \hat{M}(\boldsymbol{x}, s) + \zeta(\boldsymbol{x}) \hat{M}(\boldsymbol{x}, s) = 0 \qquad \text{for} \quad \boldsymbol{x} \in \partial\mathcal{D}, \quad s \in \mathbb{C}, \quad \mathrm{Re}(s) > 0, \tag{12}$$

respectively. The problem as defined for $\hat{M}(\boldsymbol{x}, s)$ has, for $\mathrm{Re}(s) > 0$, a unique solution. Once this solution has been constructed, $M(\boldsymbol{x}, t)$ follows from the Bromwich integral representation

$$M(\boldsymbol{x}, t) = \frac{1}{2\pi \mathrm{i}} \int_{s \in \mathcal{B}} \exp(st) \hat{M}(\boldsymbol{x}, s) \, \mathrm{d}s, \tag{13}$$

where $\mathcal{B}$ is any path parallel to the imaginary s-axis in the right half of the complex s-plane, in which half-plane $\hat{M}(\boldsymbol{x}, s)$ is an analytic function of s.

3. The natural decay rates and their associated diffusive field constituents

Since $\hat{M}(\boldsymbol{x}, s)$ is analytic in the right half of the complex s-plane, it admits an analytic continuation into the left half of the complex s-plane. In this procedure, we encounter the singularities of $\hat{M}(\boldsymbol{x}, s)$. We assume that these consist of a denumerable set of simple poles $\{s_n; n = 1, 2, 3, \ldots\}$ with $\mathrm{Re}(s_n) < 0$, which we assume to be ordered such that $\mathrm{Re}(s_{n+1}) < \mathrm{Re}(s_n)$. As a consequence, we can write $\hat{M}(\boldsymbol{x}, s)$ as the partial-fraction representation

$$\hat{M}(\boldsymbol{x}, s) = \sum_{n=1}^{\infty} \frac{M_n(\boldsymbol{x})}{s - s_n}, \tag{14}$$

where

$$M_n(\boldsymbol{x}) = \mathrm{Residue}_{s=s_n} \hat{M}(\boldsymbol{x}, s). \tag{15}$$

Upon supplementing, for $t > 0$, the Bromwich path in equation (13) with a semi-circular arc at infinity to the left, the application of Jordan's lemma and the theory of residues leads to the modal representation

$$M(\boldsymbol{x}, t) = \left[\sum_{n=1}^{\infty} M_n(\boldsymbol{x}) \exp(s_n t) \right] H(t) \qquad \text{for} \quad \boldsymbol{x} \in \mathcal{D}, \tag{16}$$

where $H(t)$ is the Heaviside unit step function. In the standard eigenvalue theory of diffusive initial-value problems in a restricted region, the sequence $\{s_n; n = 1, 2, 3, \ldots\}$ is denoted as the sequence of the *natural decay rates*.

Now, $M(\boldsymbol{x}, t)$ as given by equation (16) can, in view of equations (3) and (9), be conceived of as arising from the Laplace transformation of

$$\nabla \cdot [\overleftrightarrow{D}(\boldsymbol{x}) \cdot \nabla M(\boldsymbol{x}, t)] - \beta(\boldsymbol{x}) M(\boldsymbol{x}, t) - \partial_t M(\boldsymbol{x}, t) = -M_0(\boldsymbol{x}) \delta(t) \qquad \text{for} \quad \boldsymbol{x} \in \mathcal{D}, \tag{17}$$

where $\delta(t)$ denotes the Dirac delta distribution operative at $t = 0$. Substitution of equation (16) into equation (17) leads to

$$\sum_{n=1}^{\infty} [\nabla \cdot [\overleftrightarrow{D}(\boldsymbol{x}) \cdot \nabla M_n(\boldsymbol{x})] - \beta(\boldsymbol{x}) M_n(\boldsymbol{x}) - s_n M_n(\boldsymbol{x})] \exp(s_n t) = 0$$
$$\text{for} \quad \boldsymbol{x} \in \mathcal{D}, \quad t > 0. \tag{18}$$

By multiplying through successively by $\exp(-s_1 t)$, $\exp(-s_2 t)$, $\exp(-s_3 t)$, ..., and taking the limit $t \to \infty$, it follows that $M_n(\boldsymbol{x})$ must, for $n = 1, 2, 3, \ldots$, satisfy the relation

$$\nabla \cdot [\overleftrightarrow{D}(\boldsymbol{x}) \cdot \nabla M_n(\boldsymbol{x})] - \beta(\boldsymbol{x}) M_n(\boldsymbol{x}) - s_n M_n(\boldsymbol{x}) = 0 \qquad \text{for} \quad \boldsymbol{x} \in \mathcal{D}, \quad n = 1, 2, 3, \ldots. \tag{19}$$

The application of a similar procedure to the boundary conditions (10)–(12) leads to

Dirichlet problem:

$$M_n(\boldsymbol{x}) = 0 \qquad \text{for} \quad \boldsymbol{x} \in \partial\mathcal{D}, \quad n = 1, 2, 3, \ldots, \tag{20}$$

Neumann problem:

$$\boldsymbol{\nu}(\boldsymbol{x}) \cdot \overleftrightarrow{\boldsymbol{D}}(\boldsymbol{x}) \cdot \nabla M_n(\boldsymbol{x}) = 0 \qquad \text{for} \quad \boldsymbol{x} \in \partial\mathcal{D}, \quad n = 1, 2, 3, \ldots \tag{21}$$

and

Robin problem:

$$\boldsymbol{\nu}(\boldsymbol{x}) \cdot \overleftrightarrow{\boldsymbol{D}}(\boldsymbol{x}) \cdot \nabla M_n(\boldsymbol{x}) + \zeta(\boldsymbol{x}) M_n(\boldsymbol{x}) = 0 \qquad \text{for} \quad \boldsymbol{x} \in \partial\mathcal{D}, \quad n = 1, 2, 3, \ldots. \tag{22}$$

So far, the sequence of functions $\{M_1(\boldsymbol{x}), M_2(\boldsymbol{x}), M_3(\boldsymbol{x}), \ldots\}$ is dependent on the initial field distribution $M_0(\boldsymbol{x})$ out of which they have been constructed. However, equations (19)–(22) have the structure of a standard eigenvalue problem, associated with the differential equation (19), in combination with either of the boundary conditions (20)–(22). The properties of the eigenvalues and the corresponding eigenfunctions of this eigenvalue problem are the subject of investigation in the following section.

4. The eigenvalue problem associated with the natural decay rates of eigenmodes in the cavity

Let the sequence of eigenfunctions associated with the sequence of eigenvalues $\{s_1, s_2, s_3, \ldots\}$ be denoted by $\{\phi_1(\boldsymbol{x}), \phi_2(\boldsymbol{x}), \phi_3(\boldsymbol{x}), \ldots\}$. Then,

$$\nabla \cdot [\overleftrightarrow{\boldsymbol{D}}(\boldsymbol{x}) \cdot \nabla \phi_n(\boldsymbol{x})] - \beta(\boldsymbol{x}) \phi_n(\boldsymbol{x}) - s_n \phi_n(\boldsymbol{x}) = 0 \qquad \text{for} \quad \boldsymbol{x} \in \mathcal{D}, \quad n = 1, 2, 3, \ldots. \tag{23}$$

and

Dirichlet problem:

$$\phi_n(\boldsymbol{x}) = 0 \qquad \text{for} \quad \boldsymbol{x} \in \partial\mathcal{D}, \quad n = 1, 2, 3, \ldots \tag{24}$$

Neumann problem:

$$\boldsymbol{\nu}(\boldsymbol{x}) \cdot \overleftrightarrow{\boldsymbol{D}}(\boldsymbol{x}) \cdot \nabla \phi_n(\boldsymbol{x}) = 0 \qquad \text{for} \quad \boldsymbol{x} \in \partial\mathcal{D}, \quad n = 1, 2, 3, \ldots \tag{25}$$

and

Robin problem:

$$\boldsymbol{\nu}(\boldsymbol{x}) \cdot \overleftrightarrow{\boldsymbol{D}}(\boldsymbol{x}) \cdot \nabla \phi_n(\boldsymbol{x}) + \zeta(\boldsymbol{x}) \phi_n(\boldsymbol{x}) = 0 \qquad \text{for} \quad \boldsymbol{x} \in \partial\mathcal{D}, \quad n = 1, 2, 3, \ldots. \tag{26}$$

A first relation is obtained by multiplying through in equation (23) by $\phi_n^*(\boldsymbol{x})$, where * denotes complex conjugate, integrating over the domain $\mathcal{D}$, and applying the divergence theorem. This leads to

$$\int_{\partial\mathcal{D}} \phi_n^* \boldsymbol{\nu} \cdot \overleftrightarrow{\boldsymbol{D}} \cdot \nabla \phi_n \, \mathrm{d}A - \int_{\mathcal{D}} \nabla \phi_n^* \cdot \overleftrightarrow{\boldsymbol{D}} \cdot \nabla \phi_n \, \mathrm{d}V - \int_{\mathcal{D}} \beta \phi_n^* \phi_n \, \mathrm{d}V - s_n \int_{\mathcal{D}} \phi_n^* \phi_n \, \mathrm{d}V = 0. \tag{27}$$

Using in the first term on the left-hand side either of the boundary conditions (24)–(26), it follows that s_n is real and negative for all $n = 1, 2, 3, \ldots$. On account of this we can,

without loss of generality, take the functions $\phi_n(\boldsymbol{x})$ to be real valued and, accordingly, replace equation (27) by

$$\int_{\partial\mathcal{D}} \phi_n \boldsymbol{\nu} \cdot \overleftrightarrow{\boldsymbol{D}} \cdot \nabla\phi_n \, \mathrm{d}A - \int_{\mathcal{D}} \nabla\phi_n \cdot \overleftrightarrow{\boldsymbol{D}} \cdot \nabla\phi_n \, \mathrm{d}V - \int_{\mathcal{D}} \beta\phi_n\phi_n \, \mathrm{d}V - s_n \int_{\mathcal{D}} \phi_n\phi_n \, \mathrm{d}V = 0. \quad (28)$$

Equation (28) serves as the basis for the investigation into the variational properties of the natural decay rates to be discussed in the following section. Employing the relevant boundary conditions, equation (28) yields, for the three boundary-value problems under consideration,

Dirichlet and Neumann problems:

$$\int_{\mathcal{D}} \nabla\phi_n \cdot \overleftrightarrow{\boldsymbol{D}} \cdot \nabla\phi_n \, \mathrm{d}V + \int_{\mathcal{D}} \beta\phi_n\phi_n \, \mathrm{d}V + s_n \int_{\mathcal{D}} \phi_n\phi_n \, \mathrm{d}V = 0 \quad (29)$$

and

Robin problem:

$$\int_{\partial\mathcal{D}} \zeta\phi_n\phi_n \, \mathrm{d}A + \int_{\mathcal{D}} \nabla\phi_n \cdot \overleftrightarrow{\boldsymbol{D}} \cdot \nabla\phi_n \, \mathrm{d}V + \int_{\mathcal{D}} \beta\phi_n\phi_n \, \mathrm{d}V + s_n \int_{\mathcal{D}} \phi_n\phi_n \, \mathrm{d}V = 0. \quad (30)$$

Note that the Dirichlet and Neumann problems lead to the same equations.

5. Variational properties of the natural decay rates

To establish the variational properties of the natural decay rates, we replace, in equations (29) and (30), $\phi_n(\boldsymbol{x})$ by $\phi_n + \epsilon v_n(\boldsymbol{x})$, where $v_n(\boldsymbol{x})$ is an arbitrary piecewise continuous function defined on $\mathcal{D} \cup \partial\mathcal{D}$ and piecewise continuously differentiable in $\mathcal{D}$, while ϵ is a variational parameter. The equality sign in the resulting expressions is preserved by replacing s_n by $s_n + \delta s_n$. Under this procedure, equations (29) and (30) are replaced by

Dirichlet and Neumann problems:

$$\int_{\mathcal{D}} \nabla(\phi_n + \epsilon v_n) \cdot \overleftrightarrow{\boldsymbol{D}} \cdot \nabla(\phi_n + \epsilon v_n) \, \mathrm{d}V + \int_{\mathcal{D}} \beta(\phi_n + \epsilon v_n)(\phi_n + \epsilon v_n) \, \mathrm{d}V + (s_n + \delta s_n) \int_{\mathcal{D}} (\phi_n + \epsilon v_n)(\phi_n + \epsilon v_n) \, \mathrm{d}V = 0 \quad (31)$$

and

Robin problem:

$$\int_{\partial\mathcal{D}} \zeta(\phi_n + \epsilon v_n)(\phi_n + \epsilon v_n) \, \mathrm{d}A + \int_{\mathcal{D}} \nabla(\phi_n + \epsilon v_n) \cdot \overleftrightarrow{\boldsymbol{D}} \cdot \nabla(\phi_n + \epsilon v_n) \, \mathrm{d}V + \int_{\mathcal{D}} \beta(\phi_n + \epsilon v_n)(\phi_n + \epsilon v_n) \, \mathrm{d}V + (s_n + \delta s_n) \int_{\mathcal{D}} (\phi_n + \epsilon v_n)(\phi_n + \epsilon v_n) \, \mathrm{d}V = 0, \quad (32)$$

respectively. Subsequently, we employ the relation

$$\begin{aligned} \int_{\mathcal{D}} \nabla\phi_n \cdot \overleftrightarrow{\boldsymbol{D}} \cdot \nabla v_n \, \mathrm{d}V &= \int_{\mathcal{D}} \nabla \cdot (v_n \overleftrightarrow{\boldsymbol{D}} \cdot \nabla\phi_n) \, \mathrm{d}V - \int_{\mathcal{D}} v_n \nabla \cdot (\overleftrightarrow{\boldsymbol{D}} \cdot \nabla\phi_n) \, \mathrm{d}V \\ &= \int_{\partial\mathcal{D}} v_n \boldsymbol{\nu} \cdot (\overleftrightarrow{\boldsymbol{D}} \cdot \nabla\phi_n) \, \mathrm{d}A - \int_{\mathcal{D}} \beta v_n\phi_n \, \mathrm{d}V - s_n \int_{\mathcal{D}} v_n\phi_n \, \mathrm{d}V, \end{aligned} \quad (33)$$

where, successively, a vector identity, the divergence theorem and equation (23) have been used. With the aid of equations (25), (29)–(33), it then follows that

Dirichlet problem:

$$\epsilon^2 \int_{\mathcal{D}} \nabla v_n \cdot \overleftrightarrow{\boldsymbol{D}} \cdot \nabla v_n \, \mathrm{d}V + \epsilon^2 \int_{\mathcal{D}} \beta v_n v_n \, \mathrm{d}V + \epsilon^2 s_n \int_{\mathcal{D}} v_n v_n \, \mathrm{d}V + \delta s_n \int_{\mathcal{D}} (\phi_n + \epsilon v_n)(\phi_n + \epsilon v_n) \, \mathrm{d}V = 0$$
$$\text{provided that } v_n = 0 \qquad \text{for} \qquad \boldsymbol{x} \in \partial\mathcal{D}, \tag{34}$$

Neumann problem:

$$\epsilon^2 \int_{\mathcal{D}} \nabla v_n \cdot \overleftrightarrow{\boldsymbol{D}} \cdot \nabla v_n \, \mathrm{d}V + \epsilon^2 \int_{\mathcal{D}} \beta v_n v_n \, \mathrm{d}V + \epsilon^2 s_n \int_{\mathcal{D}} v_n v_n \, \mathrm{d}V + \delta s_n \int_{\mathcal{D}} (\phi_n + \epsilon v_n)(\phi_n + \epsilon v_n) \, \mathrm{d}V = 0 \tag{35}$$

and

Robin problem:

$$\epsilon^2 \int_{\partial\mathcal{D}} \zeta v_n v_n \, \mathrm{d}A + \epsilon^2 \int_{\mathcal{D}} \nabla v_n \cdot \overleftrightarrow{\boldsymbol{D}} \cdot \nabla v_n \, \mathrm{d}V + \epsilon^2 \int_{\mathcal{D}} \beta v_n v_n \, \mathrm{d}V + \epsilon^2 s_n \int_{\mathcal{D}} v_n v_n \, \mathrm{d}V + \delta s_n \int_{\mathcal{D}} (\phi_n + \epsilon v_n)(\phi_n + \epsilon v_n) \, \mathrm{d}V = 0. \tag{36}$$

Since the factor multiplying δs_n is of order $O(1)$ as $\epsilon \to 0$, it follows that δs_n is of order $O(\epsilon^2)$ as $\epsilon \to 0$. This implies that the expressions for s_n resulting from (29) and (30) are stationary in the sense of the calculus of variations. This stationarity feature can be exploited in a computational procedure aimed to determine the natural decay rates and their associated modal diffusive field distributions. Furthermore, since in equations (33)–(35) the factor multiplying δs_n is positive, while the sum of the coefficients multiplying ϵ^2 can be either positive or negative, depending on the chosen comparison function v_n (note that $s_n < 0$), δs_n for $\epsilon \neq 0$ can be either positive or negative, which implies that the stationary expressions for s_n are of a saddle-point nature.

6. Computational implementation of the variational expressions

The computational implementation of the variational expressions (34)–(36) uses a suitable sequence of basis functions $\{\psi_p(\boldsymbol{x}); p = 1, \ldots, N\}$ each member of which satisfies the conditions laid upon the variational comparison functions $v_n(\boldsymbol{x})$. Tentatively, $\phi_n(\boldsymbol{x})$ is represented as

$$\phi_n(\boldsymbol{x}) = \sum_{p=1}^{N} \xi_p^{(n)} \psi_p(\boldsymbol{x}) \qquad \text{for} \quad \boldsymbol{x} \in \mathcal{D}. \tag{37}$$

This expansion is substituted into equations (29) and (30). With the notations

$$A_{pq} = \int_{\mathcal{D}} \psi_p \psi_q \, \mathrm{d}V, \tag{38}$$

$$B_{pq} = \int_{\mathcal{D}} \nabla \psi_p \cdot \overleftrightarrow{\boldsymbol{D}} \cdot \nabla \psi_q \mathrm{d}V + \int_{\mathcal{D}} \beta \psi_p \psi_q \mathrm{d}V \tag{39}$$

and

$$C_{pq} = \int_{\partial\mathcal{D}} \zeta \psi_p \psi_q \, \mathrm{d}V, \tag{40}$$

this leads to (employing standard matrix notation)

Dirichlet problem:

$$\boldsymbol{\xi}^{(n)} \cdot \boldsymbol{B} \cdot \boldsymbol{\xi}^{(n)} + s_n^{(N)} \boldsymbol{\xi}^{(n)} \cdot \boldsymbol{A} \cdot \boldsymbol{\xi}^{(n)} = 0 \qquad \text{provided that} \quad \psi_n(\boldsymbol{x}) = 0 \quad \text{for} \quad \boldsymbol{x} \in \partial\mathcal{D}, \tag{41}$$

Neumann problem:

$$\boldsymbol{\xi}^{(n)} \cdot \boldsymbol{B} \cdot \boldsymbol{\xi}^{(n)} + s_n^{(N)} \boldsymbol{\xi}^{(n)} \cdot \boldsymbol{A} \cdot \boldsymbol{\xi}^{(n)} = 0 \tag{42}$$

and

Robin problem:

$$\boldsymbol{\xi}^{(n)} \cdot (\boldsymbol{B} + \boldsymbol{C}) \cdot \boldsymbol{\xi}^{(n)} + s_n^{(N)} \boldsymbol{\xi}^{(n)} \cdot \boldsymbol{A} \cdot \boldsymbol{\xi}^{(n)} = 0, \tag{43}$$

where the vector $\boldsymbol{\xi}^{(n)}$ contains the elements $\{\xi_p^{(n)}; p = 1, \ldots, N\}$. Applying arbitrary variations to the expansion coefficients $\xi_p^{(n)}$ and imposing the condition that equations (41)–(43) be stationary under these variations, we are led to the relations

Dirichlet problem:

$$\boldsymbol{B} \cdot \boldsymbol{\xi}^{(n)} + s_n^{(N)} \boldsymbol{A} \cdot \boldsymbol{\xi}^{(n)} = 0 \qquad \text{provided that} \quad \psi_n(\boldsymbol{x}) = \boldsymbol{0} \qquad \text{for} \quad \boldsymbol{x} \in \partial\mathcal{D}, \tag{44}$$

Neumann problem:

$$\boldsymbol{B} \cdot \boldsymbol{\xi}^{(n)} + s_n^{(N)} \boldsymbol{A} \cdot \boldsymbol{\xi}^{(n)} = \boldsymbol{0} \tag{45}$$

and

Robin problem:

$$(\boldsymbol{B} + \boldsymbol{C}) \cdot \boldsymbol{\xi}^{(n)} + s_n^{(N)} \boldsymbol{A} \cdot \boldsymbol{\xi}^{(n)} = \boldsymbol{0}. \tag{46}$$

The values of $s_n^{(N)}$ are obtained as the eigenvalues of the pertaining linear equations. All matrices occurring in equations (44)–(46) are positive definite. The values $-s_n^{(N)}$ are the natural decay rates that we are after.

7. Orthogonality properties and the completeness relation of the eigenfunctions

The eigenfunctions show certain orthogonality properties and a completeness relation that will now be discussed.

Upon multiplying equation (23), satisfied by $\phi_n(\boldsymbol{x})$, by $\phi_m(\boldsymbol{x})$, multiplying the corresponding equation satisfied by $\phi_m(\boldsymbol{x})$ by $\phi_n(\boldsymbol{x})$, integrating the resulting two equations over $\mathcal{D}$, applying the divergence theorem, using the pertaining boundary conditions on $\partial\mathcal{D}$ and subtracting the results, we obtain

$$(s_m - s_n) \int_{\mathcal{D}} \phi_m(\boldsymbol{x}) \phi_n(\boldsymbol{x}) \, \mathrm{d}V = 0. \tag{47}$$

This yields the orthogonality relation

$$\int_{\mathcal{D}} \phi_m(\boldsymbol{x}) \phi_n(\boldsymbol{x}) \, \mathrm{d}V = 0 \qquad \text{for} \quad s_m \neq s_n. \tag{48}$$

In the remainder of our analysis we shall assume that $s_m \neq s_n$ for $m \neq n$, i.e., the sequence of eigenvalues is assumed to be non-degenerate. Using the sequence of eigenfunctions as a sequence of expansion functions for the solution to equation (9), we employ the Ansatz

$$\hat{M}(\boldsymbol{x}, s) = \sum_{m=1}^{\infty} \alpha_m(s)\phi_m(\boldsymbol{x}) \qquad \text{for} \quad \boldsymbol{x} \in \mathcal{D}. \tag{49}$$

Upon multiplying equation (9) by $\phi_n(\boldsymbol{x})$, multiplying equation (23) by $\hat{M}(\boldsymbol{x}, s)$, integrating the two resulting equations over $\mathcal{D}$, applying the divergence theorem, using the pertaining boundary conditions on $\partial\mathcal{D}$ and subtracting the results, we obtain

$$(s - s_n) \int_{\mathcal{D}} \phi_n(\boldsymbol{x})\hat{M}(\boldsymbol{x}, s)\, \mathrm{d}V = \int_{\mathcal{D}} \phi_n(\boldsymbol{x})M_0(\boldsymbol{x})\, \mathrm{d}V. \tag{50}$$

Substituting into this relation expansion (49) and using the orthogonality relation (48), we end up with

$$(s - s_n)\alpha_n(s) \int_{\mathcal{D}} \phi_n(\boldsymbol{x})\phi_n(\boldsymbol{x})\, \mathrm{d}V = \int_{\mathcal{D}} \phi_n(\boldsymbol{x})M_0(\boldsymbol{x})\, \mathrm{d}V, \tag{51}$$

from which it follows that

$$\alpha_n(s) = \frac{1}{s - s_n} \frac{\int_{\mathcal{D}} \phi_n(\boldsymbol{x})M_0(\boldsymbol{x})\, \mathrm{d}V}{\int_{\mathcal{D}} \phi_n(\boldsymbol{x})\phi_n(\boldsymbol{x})\, \mathrm{d}V}. \tag{52}$$

Using this expression in equation (49) and writing the result as

$$\hat{M}(\boldsymbol{x}, s) = \int_{\mathcal{D}} \hat{G}(\boldsymbol{x}, \boldsymbol{x}', s)M_0(\boldsymbol{x}')\, \mathrm{d}V(\boldsymbol{x}'), \tag{53}$$

where $\hat{G}(\boldsymbol{x}, \boldsymbol{x}', s)$ is the pertaining s-domain Green function (or propagator [2]) that satisfies

$$\nabla \cdot [\overleftrightarrow{\boldsymbol{D}}(\boldsymbol{x}) \cdot \nabla \hat{G}(\boldsymbol{x}, \boldsymbol{x}', s)] - \beta(\boldsymbol{x})\hat{G}(\boldsymbol{x}, \boldsymbol{x}', s) - s\hat{G}(\boldsymbol{x}, \boldsymbol{x}', s) = -\delta(\boldsymbol{x} - \boldsymbol{x}')$$
$$\text{for} \quad \boldsymbol{x} \in \mathcal{D}, \quad \boldsymbol{x}' \in \mathcal{D}, \quad s \in \mathbb{C}, \quad \mathrm{Re}(s) > 0, \tag{54}$$

we conclude that

$$\hat{G}(\boldsymbol{x}, \boldsymbol{x}', s) = \sum_{n=1}^{\infty} \frac{1}{s - s_n} \frac{\phi_n(\boldsymbol{x})\phi_n(\boldsymbol{x}')}{\int_{\mathcal{D}} \phi_n(\boldsymbol{x}')\phi_n(\boldsymbol{x}')\, \mathrm{d}V(\boldsymbol{x}')}$$
$$\text{for} \quad \boldsymbol{x} \in \mathcal{D}, \quad \boldsymbol{x}' \in \mathcal{D}, \quad s \in \mathbb{C}, \quad \mathrm{Re}(s) > 0. \tag{55}$$

From equations (53)–(55) it follows that the corresponding time-domain result is

$$M(\boldsymbol{x}, t) = \int_{\boldsymbol{x}' \in \mathcal{D}} \int_{t'=0}^{t} G(\boldsymbol{x}, \boldsymbol{x}', t')M_0(\boldsymbol{x}')\delta(t - t')\, \mathrm{d}t'\, \mathrm{d}V(\boldsymbol{x}')$$
$$= \int_{\boldsymbol{x}' \in \mathcal{D}} G(\boldsymbol{x}, \boldsymbol{x}', t)M_0(\boldsymbol{x}')\, \mathrm{d}V(\boldsymbol{x}'), \tag{56}$$

where $G(\boldsymbol{x}, \boldsymbol{x}', t')$ is the initial-value Green function satisfying

$$\nabla \cdot [\overleftrightarrow{\boldsymbol{D}}(\boldsymbol{x}) \cdot \nabla G(\boldsymbol{x}, \boldsymbol{x}', t)] - \beta(\boldsymbol{x})G(\boldsymbol{x}, \boldsymbol{x}', t) - \partial_t G(\boldsymbol{x}, \boldsymbol{x}', t) = -\delta(\boldsymbol{x} - \boldsymbol{x}')\delta(t)$$
$$\text{for} \quad \boldsymbol{x} \in \mathcal{D}, \quad \boldsymbol{x}' \in \mathcal{D}, \quad t \in \mathbb{R}, \tag{57}$$

and can be expressed as

$$G(\boldsymbol{x}, \boldsymbol{x}', t') = \left[\sum_{n=1}^{\infty} \frac{\phi_n(\boldsymbol{x})\phi_n(\boldsymbol{x}')}{\int_{\mathcal{D}} \phi_n(\boldsymbol{x})\phi_n(\boldsymbol{x})\, \mathrm{d}V} \exp(s_n t) \right] H(t). \tag{58}$$

The property that the Green function can be expressed in terms of the eigenfunctions makes the sequence of eigenfunctions a complete one [8, pp 65–8].

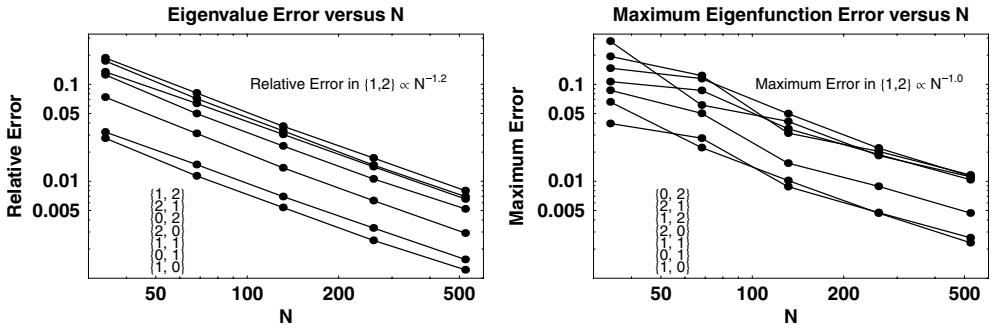

Figure 2. Relative error in the natural decay rates and their modal distributions versus the number of mesh nodes N for the rectangular-domain test example. The modal distributions are normalized to unit amplitude at $x_1 = 0, x_2 = 0$. The natural decay rate indices of the seven plotted curves are displayed in the lower left in the same order as the left side of the curves.

8. Numerical examples

A computational implementation of the variational expressions was made for 2D and 3D models in which the domain $\mathcal{D}$ is tessellated into simplices and the eigenfunctions $\phi_n(\boldsymbol{x})$ in $\mathcal{D}$ are expanded in terms of piecewise linear basis functions.

Mesh generation was performed using the Persson and Strang algorithm [9]. This easy-to-implement algorithm produces high-quality meshes for arbitrary domains, and provides an easy mechanism for describing the domain shape in two and three dimensions, including domains with holes. The algorithm includes a mesh-refinement function that describes how the mesh size should vary in space. The qhull algorithm [10] was used within that algorithm to perform Delaunay tessellation.

The first example examines the convergence of the eigenmode solutions versus the number of mesh nodes. Each eigenmode is characterized by its eigenvalue (the negative of the decay rate) and its spatial distribution (the eigenfunction). In this example, the 2D domain $\mathcal{D}$ is taken to be the rectangle $\{0 < x_1 < L_1, 0 < x_2 < L_2\}$ with a Neumann condition on its boundary. The parameters are assigned the values $\overleftrightarrow{\boldsymbol{D}}(\boldsymbol{x}) = \overleftrightarrow{\mathbf{1}}$, where $\overleftrightarrow{\mathbf{1}}$ is the unit tensor of rank 2 (isotropic diffusion) and $\beta(\boldsymbol{x}) = 1$. The analytical solution for this problem can be found by the method of separation of variables and is obtained as

$$\begin{aligned} &s_{mn} = -1 - \pi^2\left(m^2/L_1^2 + n^2/L_2^2\right), \\ &\phi_{mn}(\boldsymbol{x}) = \cos(m\pi x_1/L_1)\cos(n\pi x_2/L_2) \qquad \text{for} \quad \{m, n = 0, 1, 2\ldots\}. \end{aligned} \tag{59}$$

For the values $L_1 = 1.1$ and $L_2 = 1$, the relative error in the natural decay rate estimates is plotted in figure 2 along with the relative maximum error in the modal distribution estimates versus the number of mesh nodes N. L_1 is taken slightly different from L_2 to avoid multiple eigenvalues (degeneracy) within the range of plotted eigenvalues. The relative errors in the computed natural decay rate all turn out to follow the curve

$$\text{relative error} \propto N^{-1.2}. \tag{60}$$

The maximum errors in the modal distributions are also found to follow a power law, be it with more variety in the exponents than the natural decay rates do. So, the power law for a representative curve, $\{m = 1, n = 2\}$, is found as

$$\text{maximum error} \propto N^{-1.0}. \tag{61}$$

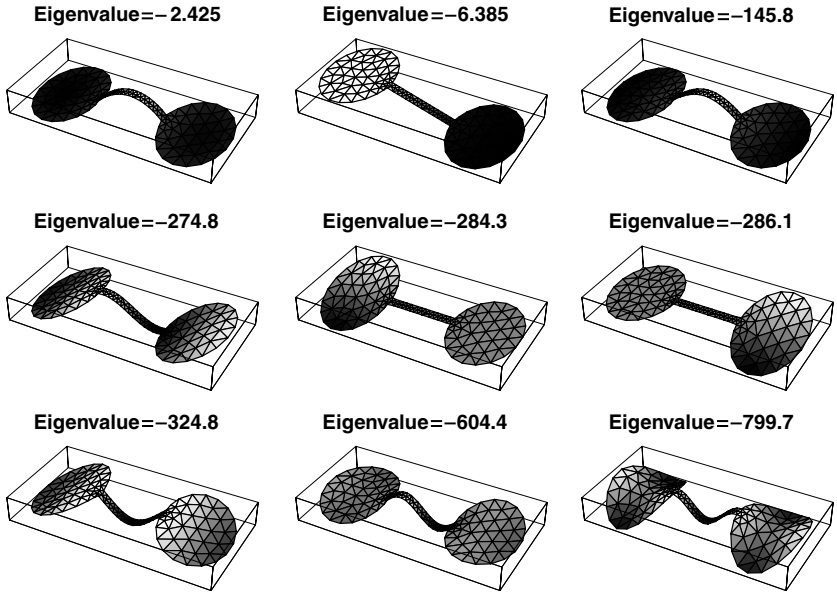

Figure 3. The first nine eigenfunctions and their eigenvalues for a two-dimensional two-pore porous material example. The horizontal axes correspond to the two spatial dimensions (to scale) and the vertical axis is the eigenfunction value. Lighter shades indicate larger eigenfunction values.

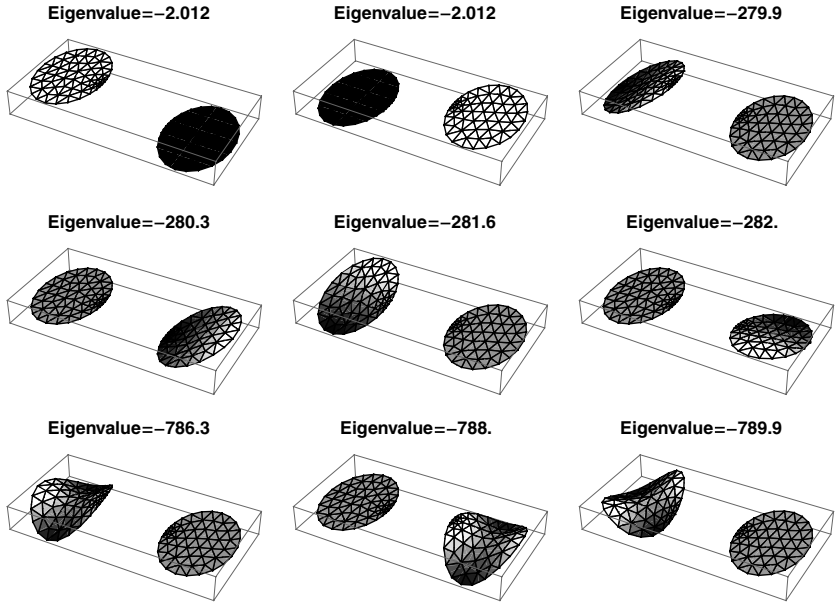

Figure 4. This is the same example as in figure 3, but with no connection between the two pores.

Using Δ to represent a characteristic length of a mesh element, N grows as Δ^{-2}. This leads to the natural decay rate error formula

$$\text{relative error} \propto \Delta^{2.4}, \tag{62}$$

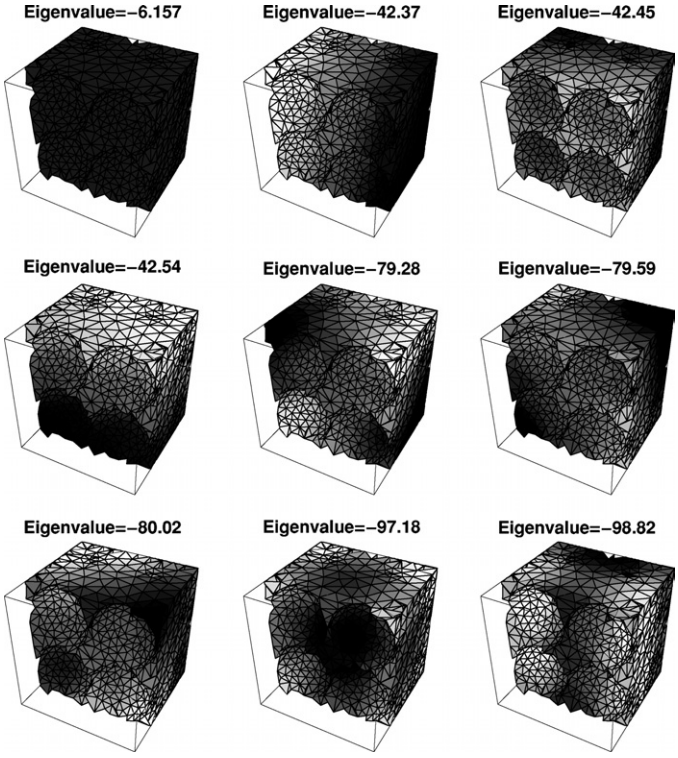

Figure 5. The first nine eigenfunctions and their eigenvalues for the third example: a 3D model with eight cubically-packed spherical pores. The interior of the cube is exposed by removing triangles whose centers lie in $0 \leqslant y \leqslant 5$. The three axes correspond to the three spatial dimensions (to scale) and the shading indicates the eigenfunction value. Lighter shades indicate larger eigenfunction values.

which indicates a better than quadratic convergence. This is slightly better than the quadratic convergence that could be expected from our variational analysis. Although our variational analysis provides no prediction as to the modal distribution convergence rate, the convergence rate in the numerical example under consideration was also found to be quadratic.

The next example is a representative of a two-dimensional porous material filled with water. Here, two circular pores of diameter 10 μm each are interconnected by a narrow channel of length 10 μm and width 1 μm. The material coefficients are $\overleftrightarrow{\boldsymbol{D}}(\boldsymbol{x}) = 2000\ \mu\text{m}^2\ \text{s}^{-1}\ \overleftrightarrow{\mathbf{1}}$, $\beta(\boldsymbol{x}) = 0$ and $\zeta(\boldsymbol{x}) = 5\ \mu\text{m s}^{-1}$. Figure 3 shows the modal distributions and their natural decay rates for the first nine eigenmodes in this example. The finite-element mesher was instructed to make the elements within the channel a factor of three smaller in linear dimension than those in the pores. Note that, because of the presence of surface relaxation, the distribution of the first eigenmode is not a constant as in our rectangular cavity example with a Neumann boundary condition. From (58) we see that larger eigenvalues correspond to shorter observation times, with the eigenmode corresponding to eigenvalue s_n decaying by $1/e$ in characteristic time $t = 1/|s_n|$. The first nine modes have characteristic times between 1.3 and 410 ms. For comparison, figure 4 shows the same example, with no channel connecting the pores. The characteristic times span roughly the same range, 1.3–500 ms, but the eigenmodes show many degenerate eigenvalues. Comparing the two sets of eigenmodes, some clearly

reflect the effects of the connectivity of the system. For example, the first two modes of the uncoupled system are degenerate. The first mode of the coupled system is very similar to the corresponding one in the uncoupled system. The second mode of the couple system exhibits an enhanced eigenvalue specifically due to the coupling. As a result, a measurement of this mode could be important for probing the connectivity of the system. In fact, other modes are also affected by the coupling, however, the effect is likely weaker for the higher modes [11].

The third example is a 3D porous material filled with water. The model is $20 \times 20 \times 20$ μm^3 with eight cubically-packed spherical rock grains of 10 μm diameter each. The material properties are the same as in the previous example. The finite-element mesher was instructed to perform a smooth transition to smaller elements near the grain contacts. The resulting eigenmodes are illustrated in figure 5. In this example, the increase in decay-rate magnitude with increasing mode number is much less rapid than in the previous one. The first nine modes have characteristic times between 10 and 160 ms. To capture characteristic times down to 1.3 ms, as in the 2D example, requires the first 59 modes, as compared to nine in the 2D case.

9. Conclusions

We have formulated a variational finite-element approach to the computation of the natural decay rates and their eigenmodes of cavity-enclosed diffusive fields for general heterogeneous, anisotropic materials and cavities of arbitrary shape and size. As to the cavity's interaction at its boundary, we consider the cases that can be modeled through either Dirichlet, or Neumann, or Robin boundary conditions. The eigenmodes are proven to be orthogonal and to form a complete sequence of expansion functions for the time-domain diffusive field. Numerical experiments demonstrate the method in two and three dimensions to be simple and robust.

The computational method based on our variational analysis is a promising tool for the recurrent generation of solutions to the forward problem for cavity-enclosed diffusive fields, in the realm of the inverse problems associated with, for example, a variety of NMR imaging applications such as the structure of subsurface porous rock, biological cell structure and the analysis of neurological defects in medical diagnostics.

Acknowledgment

We wish to thank Yi-Qiao Song of Schlumberger-Doll Research for his contributions and careful review of this document.

References

[1] Sen P B 2004 Time-dependent diffusion coefficient as a probe of geometry *Concepts Magn. Reson.* A **23** 1–21
[2] Song Y-Q 2003 Using internal magnetic fields to obtain pore size distributions of porous media *Concepts Magn. Reson.* A **18** 97–110
[3] Brownstein K R and Tarr C E 1979 Importance of classical diffusion in NMR studies of water in biological cells *Phys. Rev.* A **19** 2446–53
[4] Crank J 1975 *The Mathematics of Diffusion* (Oxford: Clarendon) chapters 5 and 6
[5] Sen P N, André A and Axelrod S 1999 Spin echoes of nuclear magnetization diffusing in a constant magnetic field gradient and in a restricted geometry *J. Chem. Phys.* **111** 6548–55
[6] Torrey H C 1956 Bloch equations with diffusion terms *Phys. Rev.* **104** 563–5
[7] Song Y-Q, Ryu S and Sen P N 2000 Determining multiple length scales in rocks *Nature* **406** 178–81

[8] Hochstadt H 1973 *Integral Equations* (New York: Wiley)
[9] Persson P-O and Strang G 2004 A simple mesh generator in MATLAB *SIAM Rev.* **46** 329–45
[10] Barber C B, Dobkin D P and Huhdanpaa H 1996 The quickhull algorithm for convex hulls *ACM Trans. Math. Softw.* **22** 469–83
[11] Zielinski L, Song Y-Q, Ryu S and Sen P N 2002 Characterization of coupled pore systems from the diffusion eigenspectrum *J. Chem. Phys.* **117** 5361–5